Dynamical Gauge Fields with Bosonic Codes

Javier del Pino[1,*] and Oded Zilberberg[2]
[1]Institute for Theoretical Physics, ETH Zürich, 8093 Zürich, Switzerland
[2]Department of Physics, University of Konstanz, 78464 Konstanz, Germany

(Received 22 November 2022; revised 31 March 2023; accepted 4 April 2023; published 27 April 2023)

The quantum simulation of dynamical gauge field theories offers the opportunity to study complex high-energy physics with controllable low-energy devices. For quantum computation, bosonic codes promise robust error correction that exploits multiparticle redundancy in bosons. Here, we demonstrate how bosonic codes can be used to simulate dynamical gauge fields. We encode both matter and dynamical gauge fields in a network of resonators that are coupled via three-wave mixing. The mapping to a $\mathbb{Z}_2$ dynamical lattice gauge theory is established when the gauge resonators operate as Schrödinger cat states. We explore the optimal conditions under which the system preserves the required gauge symmetries. Our findings promote realizing high-energy models using bosonic codes.

DOI: 10.1103/PhysRevLett.130.171901

Dynamical gauge field theories (DGFTs), commonly appearing in high-energy physics, are extremely challenging to simulate or solve using classical methods. A prototypical example is quantum electrodynamics, a theory that features "matter" degrees of freedom interacting in the presence of "light" gauge fields. The two constituents experience complex combined dynamics, e.g., via the change in the electric field caused by the redistribution of charges. The gauge fields in electrodynamics are Abelian, i.e., their quantum operators commute. In this "simple" DGFT, we have a continuous U(1) degree of freedom with evolution in an infinite-dimensional Hilbert space. In other realms, even more complex DGFTs appear, e.g., in quantum chromodynamics, where they describe quark-gluon interactions in heavy-ion collisions, or the deep core of neutron stars [1,2].

In recent years, quantum simulators have become a reality, leading to the emulation of numerous effects, such as topological phases of matter [3–7], collective phenomena [8–10], cascade effects [11,12], and many more. Such technologies also offer the means to controllably realize DGFTs [13–16]. The simulation relies on mapping DGFTs to simplified lattice gauge theories [17] (LGTs). This map involves confining the matter degrees of freedom to move only between nodes of a lattice, while the gauge fields are associated with the links between the nodes [17,18]. Further simplifications involve using low-dimensional "quantum links" that replace infinite-dimensional gauge fields, while preserving the symmetries of the original model [13,37,38]. In addition, minimal $\mathbb{Z}_2$-symmetric LGTs appeared and have sparked interest in spin [17], fermionic [39], and bosonic models [40], as well as the toric code for quantum error correction [41].

The quantum simulation of DGFTs, however, is very challenging. Most proposals thus far harness "static" gauge fields, which act on the matter without reacting, and strive to make them dynamic [42–45]. The static fields are an established instrument for breaking spatiotemporal symmetries used to induce nontrivial topological phenomena in lattice systems [46–51]. Rendering gauge fields dynamic, LGT simulators are being developed in various quantum simulation technologies [13,15,52–66]. While the ultimate aim is to tackle more complex schemes, the current focus of the community is on implementing minimal LGT models with $\mathbb{Z}_2$ or U(1) symmetries. Yet, despite the variety of proposals, the constraints that LGTs must fulfill impede a clear experimental realization, limiting most proposals to the control of a single or few links.

Recently, bosonic error correction codes have spurred much interest as a possible route for robust and scalable quantum computing [67–71]. These codes exploit the infinite-dimensional Hilbert space of a harmonic oscillator for redundant information encoding, thus significantly reducing hardware requirements (see the Supplemental Material [18]). Remarkably, the realization of the so-called cat qubit, the workhorse of bosonic codes [72], has been recently proposed and demonstrated in nonlinear microwave cavities [73–76]. A wide variety of platforms could potentially allow for bosonic cat codes, including cavity QED [77], trapped ions [78], bulk acoustic-wave resonators [79], nanomechanical [80], and optomechanical [81] systems. The prospects for error correction make bosonic code platforms an interesting candidate also for quantum simulation (see the Supplemental Material [18]).

In this Letter, we demonstrate how a $\mathbb{Z}_2$ LGT can be realized using a bosonic code setup. Specifically, we consider a coupled resonator network whose nodes embody both matter and gauge fields. The gauge resonators are nonlinear and driven into "Schrödinger cat" states that encode the dynamical gauge fields. Three-wave mixing

between the network resonators engenders a gauge-invariant light-matter coupling. We explore the bounds for the ideal operation of our scheme and show that it requires the cat states to have a finite coherent amplitude and the three-wave mixing to be moderate. In this regime, we obtain similar functionality and scaling strategies as contemporarily used in standard-qubit-based LGTs [14,16]. Concurrently, we benefit from the substantial advantage of bosonic codes compared with qubit-based approaches, e.g., their reduced hardware overhead due to efficient quantum-error correction. Furthermore, a compact simulator assembled using our scheme can be realized with various platforms, including photons, phonons, magnons, and polaritons.

We consider a 1D chain of coupled resonators; see Fig. 1(a). The resonators are alternatively positioned with matter nodes and gauge sites. The latter will act as links in the following. The chain's building block is a matter-field link, [labeled sites in Fig. 1(a)] governed by the Hamiltonian

$$H = H_{\text{matter}} + H_{\text{field}} + H_{\text{coup}}. \tag{1}$$

The matter nodes' Hamiltonian reads as

$$H_{\text{matter}} = \sum_{i=1,2} \omega_i a_i^\dagger a_i, \tag{2}$$

with bosonic annihilation operators a_i $(i = \{1, 2\})$ and frequency ω_i. The link's gauge site is also a resonator [cf. Eq. (5) below] with bosonic annihilation operator b,

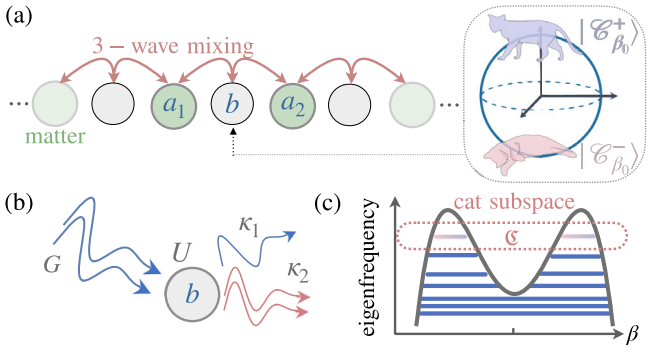

FIG. 1. (a) Chain consisting of resonators of type a and b labeled as matter and gauge modes, respectively [cf. Eq. (1)]. The resonators are coupled via three-wave mixing interactions [cf. Eq. (3)] (right zoomed box). We show that the system can simulate a $1 + 1D$ LGT when the gauge resonators are projected onto discrete bosonic code subspaces, namely, into cat states $|\mathcal{C}^\pm_{\beta_0}\rangle$ with parity $\pm$ and amplitude β_0 (see text). (b) Sketch of the "link" site as a Kerr parametric resonator [cf. Eq. (5)] subject to single- (κ_1) and two-photon (κ_2) loss. (c) The interplay between the drive G and the nonlinearity U stabilizes nonclassical states, e.g., cat states that appear as ground states of the Hamiltonian [Eq. (5)], with amplitudes β_0 that minimize the mean-field double-well potential $\langle H_{\text{field}}\rangle_{\text{MF}} = -U|\beta|^4 + G\text{Re}(\beta^2)$.

and frequency ω_b. Gauge resonators are operated in the bosonic code regime. Specifically, we assume that they operate as Schrödinger cat states, i.e., that their state is spanned by $|\mathcal{C}^\pm_\beta\rangle \sim (|\beta\rangle \pm |-\beta\rangle)$, where $|\beta\rangle$ denotes a coherent state with amplitude β [82,83]. The $\pm$ label even-odd photon number parities, where the parity operator reads as $\Pi(n) = (-1)^n$ with $n = b^\dagger b$. In the following, we define the projector $\mathcal{P}_{\mathfrak{C}} = \sum_{\eta=\pm} |\mathcal{C}^\eta_{\beta_0}\rangle\langle\mathcal{C}^\eta_{\beta_0}|$ to map our model into the bosonic code limit, where we denote the restricted "cat" Hilbert space by $\mathfrak{C}$ with ground- or steady-state cat amplitudes $\beta = \beta_0$.

The resonators b and a_i are coupled via nondegenerate three-wave mixing (3WM) [84–86],

$$H_{\text{coup}} = -g_3(a_1^\dagger b a_2 + a_2^\dagger b^\dagger a_1), \tag{3}$$

with amplitude g_3. The 3WM coupling can be realized in various ways, e.g., Raman scattering [87,88] and opto-mechanical coupling [89], and shows up as frequency conversion in nonlinear optical crystals [90,91], Josephson junctions [92], and polariton condensates [93,94]. Degenerate and nondegenerate 3WM are related by linear mode coupling [95,96].

The 3WM interaction [Eq. (3)] signifies that an excitation from a matter resonator a_i can convert into a pair of excitations that reach another matter resonator a_j, $j \neq i$ as well as the intermediate gauge resonator b, or vice versa. Hereby, "hopping" between matter sites a_i is inevitably "recorded" by an excitation arriving or leaving b, which imparts a flip in the photon-number parity $\Pi(n)$ in the gauge resonator.

Using our model [Eq. (1)], we show that a $\mathbb{Z}_2$ LGT can be realized by restricting the link resonators to evolve in their respective cat Hilbert spaces [Fig. 1(a)]. Projecting Eq. (3) onto such a subspace brings the projected Hamiltonian $H^{\mathfrak{C}}_{\text{coup}}$ into the form of a $\mathbb{Z}_2$ light-matter coupling [13]:

$$H^{\mathfrak{C}}_{\text{coup}} = -\frac{\Omega_R}{2}(a_1^\dagger L a_2 + a_2^\dagger L^\dagger a_1), \tag{4}$$

where an excitation hopping between matter nodes, with Rabi frequency $\Omega_R > 0$, is mediated by the "link" (gauge field) operator $L = \mathcal{P}_{\mathfrak{C}} b \mathcal{P}_{\mathfrak{C}}$ (see the Supplemental Material [18]). Note that $\mathcal{P}_{\mathfrak{C}}$ leaves the matter parts unaffected.

Why does our construction entail a $\mathbb{Z}_2$ LGT? In a $\mathbb{Z}_2$ LGT, (i) the gauge fields are associated with electric flux operators $E = \sigma^z$ (Pauli matrices $\{\sigma^{x,y,z}\}$), whose values change upon a redistribution of charges with operators $Q_i = (-1)^{a_i^\dagger a_i}$. This implies that the electric flux is not conserved, e.g., $L \propto \sigma^x$; (ii) the theory has a $\mathbb{Z}_2$ gauge invariance, namely the Hamiltonian maintains $H = V_i H V_i^\dagger$ for local unitary transformations $V_i = e^{i\pi\mathcal{G}_i}$, generated by operators $\mathcal{G}_i = Q_i\sigma^z$. Note that in an

extended theory, the local symmetry generators generalize to $\mathcal{G}_i = Q_i \prod_{j:\langle i,j\rangle} \sigma^z_{i,j}$, where $\sigma^z_{i,j}$ represents the gauge field on the link $\langle i,j\rangle$ in question. This is also known as the $\mathbb{Z}_2$ analog of "Gauss law," i.e., the generator is a conserved quantity $[H,\mathcal{G}_i]=0$ [13]. In our case, when we restrict the Hamiltonian to the cat space, $H_{\mathfrak{C}} = \mathcal{P}_{\mathfrak{C}} H \mathcal{P}_{\mathfrak{C}}$, we (i) recover a similar electric flux operator by also projecting the parity operation $\mathcal{P}_{\mathfrak{C}}\Pi(n+1)\mathcal{P}_{\mathfrak{C}} = \sigma^z$, where the Pauli matrices now act on the cat states $|\mathcal{C}^{\pm}_{\beta_0}\rangle$ (see the Supplemental Material [18]). Moreover, in the large cat amplitude limit, $\beta_0 \gg 1$, the gauge fields flip the parity, i.e., $L \approx \beta_0 \sigma^x$, as required. Furthermore, property (ii) then holds, leading to the invariance $H_{\mathfrak{C}} = V_i H_{\mathfrak{C}} V_i^\dagger$. The $\mathbb{Z}_2$ matter-free dynamics is introduced by a term E in $H^{\mathfrak{C}}_{\text{field}}$ [61,64], inducing rotations around the z axis $\sim\sigma_z$. While cat qubits are robust against such phase flips, several approaches to controllably generate them have been devised, e.g., in Kerr-cat qubits through pulsed–single and two-photon–drives within $\mathfrak{C}$ [97] or involving auxiliary excitations [98].

Physically, cat states can arise from the competition between two-photon driving (also known as degenerate 3WM) with Kerr nonlinearity [83] or using two-photon dissipation [99]. For instance, they manifest as the doubly degenerate ground states of a Kerr parametric oscillator (KPO) [75,76,100,101] [Fig. 1(b)]. At a rotating frame at frequency ω_b, the KPO Hamiltonian reads as

$$H_{\text{field}} = -U b^{\dagger 2} b^2 + \frac{G}{2}(b^2 + b^{\dagger 2}), \tag{5}$$

with two-photon driving amplitude G (originally at frequency $\approx 2\omega_b$), and Kerr nonlinearity U. The spectrum of the KPO [Eq. (5)] is gapped relative to the cat states with splitting approximated by $\omega_{\text{GAP}} = 4U\beta_0^2$ [75], where $\beta_0 = \sqrt{G/2U}$ [Fig. 1(c)]. The cat eigenfrequencies are degenerate at $U\beta_0^4$, such that the projected Hamiltonian simply reads as $H^{\mathfrak{C}}_{\text{field}} = U\beta_0^4 \mathbb{1}_{2\times 2}$, with a trivial zero-point frequency shift.

We turn, now, to show that the effective $\mathbb{Z}_2$ LGT $H^{\mathfrak{C}}$ well approximates the full dynamics [Eq. (1)]; see Fig. 2. We assume the gap frequency is much larger than the 3WM, $\omega_{\text{GAP}} \gg \langle H_{\text{coup}}\rangle$, and take degenerate matter sites, $\omega_1 = \omega_2$. Initially, we place a single excitation in a_1, and an even cat in b, i.e., $|\psi(t=0)\rangle = |1,\mathcal{C}^+_{\beta_0},0\rangle$. We time evolve the state using Eq. (1) with the KPO model for the gauge sites [Eq. (5)]. We observe coherent population exchange between matter modes, with Rabi frequency $\Omega_R \approx 2g_3\beta_0$, accompanied by cat parity flips. The time snapshots of the resonators' Wigner quasiprobabilities confirm that the Rabi oscillations transition between the states $|1,\mathcal{C}^+_{\beta_0},0\rangle$ and $|\psi(t=2\pi/\Omega_R)\rangle = |0,\mathcal{C}^-_{\beta_0},1\rangle$ [Fig. 2(b)].

We have shown that H implements a $\mathbb{Z}_2$ LGT when the cat amplitude β_0 is large and the 3WM is moderate. What are the limitations of our construction? We first address the

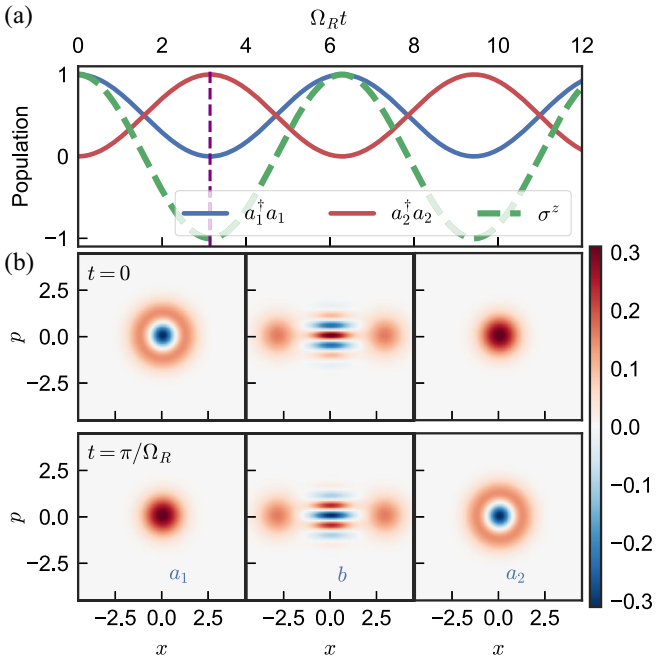

FIG. 2. (a) Light-matter population dynamics governed by the full Hamiltonian H [cf. Eq. (1)] for two matter sites coupled by a link that is realized by a KPO [cf. Eq. (5)]. The system is initiated in a state with Fock number 1 in resonator a_1, and a positive-parity Schrödinger cat state in b, denoted $|1,\mathcal{C}^+_{\beta_0},0\rangle$. The operator $\sigma^z = |\mathcal{C}^+_{\beta_0}\rangle\langle\mathcal{C}^+_{\beta_0}| - |\mathcal{C}^-_{\beta_0}\rangle\langle\mathcal{C}^-_{\beta_0}|$ returns the photon number parity for cat states within $\mathfrak{C}$. (b) Marginal Wigner functions for the three resonators at times $t=0$ and $t=\pi/\Omega_R$; the latter corresponds to the vertical dashed line in (a). The axes labels x and p denote the position and momentum for each resonator. Here $U=0.03$, $G=0.12$ ($\beta_0=2$, $\omega_{\text{GAP}}=0.48$), and $g_3=\omega_{\text{GAP}}/100$.

impact of lowering β_0, e.g., by weakening the two-photon drive $G/U \to 0$. Specifically, we repeat the procedure in Fig. 2, and extract the matrix element in H responsible for Rabi oscillations; see Fig. 3(a). We observe that, for sufficiently low β_0, a different Rabi oscillation frequency appears if we start in the odd or the even cat state (see the Supplemental Material [18]).

This difference marks a discrepancy between the light-matter interaction rates and a corresponding breakdown of the $\mathbb{Z}_2$ LGT dynamics for low β_0. It crucially originates from cat states shrinking into Fock states, $|\mathcal{C}^{\pm}_{\beta_0}\rangle \mapsto \{|0\rangle,|1\rangle\}$ as $\beta_0 \to 0$ [Fig. 3(b)]. This reduction "restores" a U(1) gauge symmetry to our model: (i) as $\beta_0 \to 0$, the Wigner functions for b go from mirror symmetric at all times to full rotationally symmetric; and (ii) the projectors in $L = \mathcal{P}_{\mathfrak{C}} b \mathcal{P}_{\mathfrak{C}}$ approximate the gauge fields to $L \sim |C^-_\beta\rangle\langle C^+_\beta|$ for $\beta_0 \ll 1$, and thus the light-matter coupling becomes invariant under arbitrary U(1) transformations [$e^{i\varphi_i \mathcal{G}_i}$ with $\varphi_i \in (0,2\pi)$] (see the Supplemental Material [18]). Moreover, the shrinking cat subspace implies that the projected states are no longer degenerate, and the time dynamics involve a distinct transition

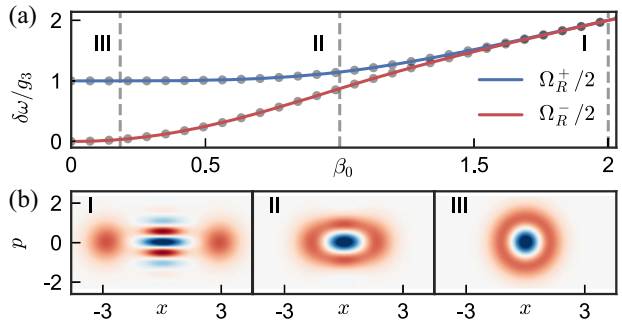

FIG. 3. (a) Matrix elements $\langle 1, \mathcal{C}^{\pm}_{\beta_0}, 0|H_{\mathfrak{C}}|0, \mathcal{C}^{\mp}_{\beta_0}, 1\rangle = \Omega^{\pm}_R/2$ of the projected Hamiltonian between opposite-parity cat states. The analytical expression for the splitting $\delta\omega$ is superimposed to the numerically exact result $\langle 1, \mathcal{C}^{\pm}_{\beta_0}, 0|H|0, \mathcal{C}^{\mp}_{\beta_0}, 1\rangle$ (gray dots). Values of β_0 in (a) are shown as dashed lines. (b) Wigner distribution of the gauge mode b, initiated in $|1, \mathcal{C}^{+}_{\beta_0}, 0\rangle$, after a full Rabi swap ($t = \pi/\Omega_R$) with decreasing amplitude $\beta_0 = 2$, 1, 0.18 along the columns. In these simulations, we choose $\Omega_R \ll \omega_{\mathrm{GAP}}$ to prevent excitation outside $\mathfrak{C}$, and take $U = 0.03$.

between Fock states. Such asymmetry reflects in the matter-field Rabi frequencies for $|1, \mathcal{C}^{+}_{\beta_0}, 0\rangle \leftrightarrow |0, \mathcal{C}^{-}_{\beta_0}, 1\rangle$ and $|1, \mathcal{C}^{-}_{\beta_0}, 0\rangle \leftrightarrow |0, \mathcal{C}^{+}_{\beta_0}, 1\rangle$ processes, which become $\Omega^{\pm}_R = 2g_3\beta_0\sqrt{(1 \pm e^{-2\beta_0^2})/(1 \mp e^{-2\beta_0^2})}$.

We now address the impact of increasing the 3WM. The procedure in Fig. 2(a) with $\langle H_{\mathrm{coup}}\rangle \sim \omega_{\mathrm{GAP}}$ and $|\psi(t=0)\rangle = |1, \mathcal{C}^{+}_{\beta_0}, 0\rangle$ [Fig. 4(a)] reveals the average electric flux beats with a reduced amplitude $\max\langle\sigma^z\rangle < 1$, and additional frequencies. This is in stark contrast with Figs. 2 and 3, where Rabi exchange at a single frequency $\Omega^{\pm}_R$ dominates the dynamics. The excitation spectrum of H also reveals an intricate structure [Fig. 4(b)], in which cat states and excitations hybridize as $\Omega^{+}_R > \omega_{\mathrm{GAP}}$. We quantify the overall hybridization of the cat states $|\mathcal{C}^{\pm}_{\beta_0}\rangle$ with the system's state $|\psi\rangle$ using the inverse participation ratio $\mathrm{IPR}_{\mathfrak{C}} = \langle\psi|\mathcal{P}_{\mathfrak{C}}|\psi\rangle^2/\langle\psi|\mathcal{P}_{\mathfrak{C}}|\psi\rangle$ [Fig. 4(c)]. The cat states delocalize over many excited states (low $\mathrm{IPR}_{\mathfrak{C}}$) as the 3WM grows and β_0 decreases. In fact, the mixing becomes relevant when $\beta_0 < g_3/(2U)$, i.e., precisely when $\Omega^{+}_R > \omega_{\mathrm{GAP}}$ [Fig. 4(d)]. Therefore, the hybridization between $\mathfrak{C}$ and $\mathfrak{C}^{\perp}$ subspaces is the cause for the multiple harmonics in Fig. 4(a) (see the Supplemental Material [18]).

Strong 3WM hybridization hampers the performance of even a single $\mathbb{Z}_2$ link. To see the extent of the deviation from a LGT, we explore how much and long the gauge symmetry, expressed by Gauss's laws $[H, \mathcal{G}_i] = 0$, is conserved. The evolution must be confined to an eigenspace of the symmetry generators $\mathcal{G}_i$ or, equivalently, the value of $\langle\mathcal{G}_i\rangle$ or "static charge" must be conserved. In the moderate 3WM limit (cf. Figs. 2 and 3) the dynamics are spanned by states $|1, \mathcal{C}^{+}_{\beta_0}, 0\rangle$ and $|0, \mathcal{C}^{-}_{\beta_0}, 1\rangle$, both of which are eigenvectors of $\mathcal{G}_i$ with static charge -1. However, for

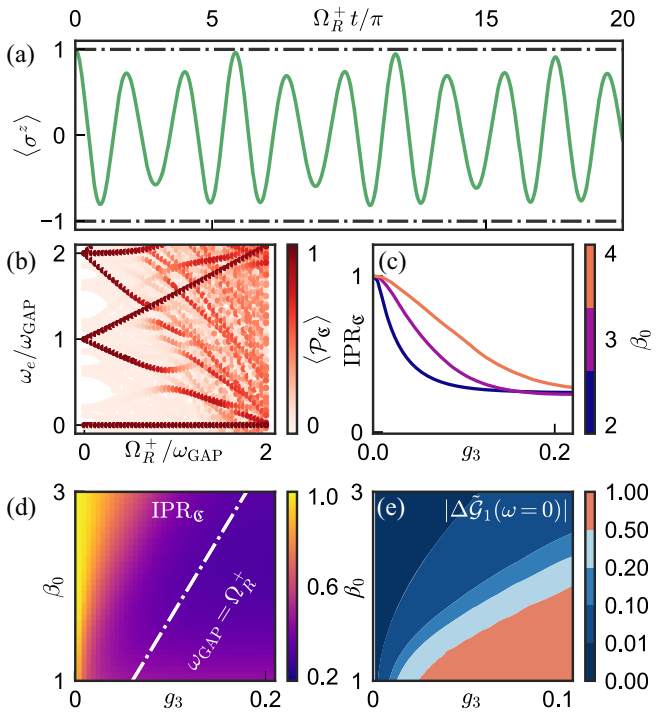

FIG. 4. (a) Evolution of $\langle\sigma^z\rangle$ for increasing 3WM. Dashed lines depict the limit where dynamics remains confined in the cat space $\mathfrak{C}$. (b) Eigenspectrum of the full Hamiltonian H for a single link $a_1 - b - a_2$. The colorscale marks the value of the projection over the cat subspace. Here and onwards, we assumed the resonance condition $\omega_i = \omega_{\mathrm{GAP}}$. (c) Inverse participation ratio for cat states in the full spectrum, where $\mathrm{IPR}_{\mathfrak{C}} = 1$ indicates full localization in $\mathfrak{C}$. (d) 2D map of $\mathrm{IPR}_{\mathfrak{C}}$ as a function of β_0 and g_3. (e) Normalized zero frequency component of $\Delta\mathcal{G}_i(t)$, marking a baseline deviation from Gauss' law. In these panels, $U = 0.03$.

large 3WM amplitudes, the dynamics from $|\psi(t=0)\rangle$ reach eigenexcitations of H with an ill-defined static charge. Similarly, hybridization causes a breakdown of Gauss's laws and produces errors in the simulation of $\mathbb{Z}_2$ light-matter dynamics. Specifically, the time-evolved operator variances $\Delta\mathcal{G}_i = \langle\mathcal{G}_i^2\rangle - \langle\mathcal{G}_i\rangle^2$, which must be zero with an eigenstate of $\mathcal{G}_i$, oscillate around a nonzero baseline. The location of this baseline, obtained from $|\Delta\tilde{\mathcal{G}}_i(\omega=0)|/\max_{J,\beta_0}[|\Delta\tilde{\mathcal{G}}_i(\omega=0)|]$ where $\Delta\tilde{\mathcal{G}}_i(\omega) = \mathrm{FT}[\Delta\mathcal{G}_i(t)]$, gives an estimate of the $\mathbb{Z}_2$ simulation error [Fig. 4(e)]. Our results reveal an ideal operation regime (errors below 1%) in the large β_0 and low g_3 region.

Until now, we examined the performance of a single bosonic code link as a building block for a $\mathbb{Z}_2$ LGT. Next, we connect two such links in a minimal $1+1D$ theory with two gauge fields linking three matter sites [Fig. 5(a)]. In Fig. 5(b), we study the dynamics initializing the system with a single matter excitation at one end of the chain. The excitation propagates from left to right while flipping the cat parity of the gauge resonators along its path, even when it bounces back off the boundary. Gauge invariance is

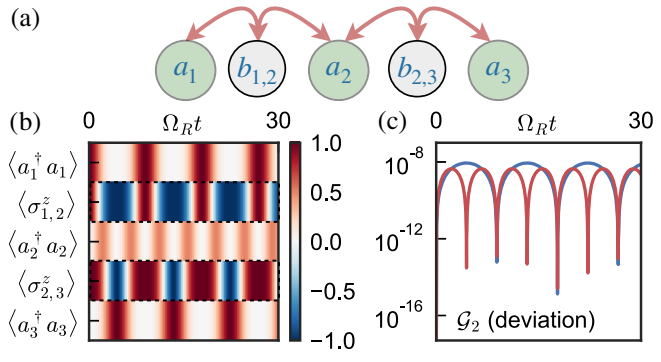

FIG. 5. (a) A small-scale $1+1D$ $\mathbb{Z}_2$ LGT with our resonator chain scheme. (b) The time evolution of resonators' populations and effective parities on cat subspaces $\mathfrak{C}_i$ starting from a single excitation in a_1. The colorscale marks $\langle a_i^\dagger a_i \rangle$ and $\langle \sigma^z_{i,i+1} \rangle$, respectively. Dashed lines separate between distinct resonator data. (c) Relative deviation of $\langle \mathcal{G}_2^{\text{chain}} \rangle$ over time. We start from an initial gauge-symmetric state, as in (b). We use $U = 0.03$, $G = 0.24$, and $g_3 = \omega_{\text{GAP}}/100$. The numerical calculations are facilitated by the truncation scheme for gauge resonators, as discussed in the text.

preserved during the evolution, as indicated by the low values of the central site relative error $|\langle \mathcal{G}_2^{\text{chain}}(t) \rangle - \langle \mathcal{G}_2^{\text{chain}}(0) \rangle| / \langle \mathcal{G}_2^{\text{chain}}(t) \rangle$ in Fig. 5(c), where $\mathcal{G}_2^{\text{chain}} = \sigma^z_{1,2} Q_2 \sigma^z_{2,3}$. Note that the system's dynamics is intrinsically tied to electric field terms $\sim \sigma^z_{i,i+1}$ and the on site repulsion on the matter sites $\sim (a_i^\dagger a_i)^2$, which we neglected here. The latter interaction terms could play a crucial role in initial state preparation, an area for future research to explore.

In the analysis of Fig. 5, we rely on truncation to the lowest M eigenstates of H_{field} instead of employing a Fock basis for b, which would require much larger truncated Hilbert spaces to properly describe cat states and their dynamics (see the Supplemental Material [18]). Since the model conserves the number of matter excitations, this reduces the dimension of the computational Hilbert space, $\mathcal{H}$, for N singly excited matter sites and $N-1$ gauge resonators to $\dim(\mathcal{H}) = NM^{N-1}$, or $\dim(\mathcal{H}) = \binom{N+N_{\text{exc}}-1}{N_{\text{exc}}} M^{N-1}$ for N_{exc} matter excitations. This method provides an accurate description of the dynamics of a chain of links. Note, however, that the exponential growth of $\dim(\mathcal{H})$ still implies that a proper description of larger systems requires the assistance of quantum simulation devices.

Our proposal motivates the realization of LGT quantum simulation using bosonic code networks. In light of contemporary results in the field [76], the realization of the basic building block of the model is within experimental reach. Note, however, that with superconducting devices, future work will need to address the interplay between the out-of-equilibrium drives and dissipation for a more realistic description. Nevertheless, with the abundance of new bosonic code platforms available, the Hamiltonian description presented here is sufficiently broad to inspire LGT emulation in other systems. The natural redundancy in bosonic Hilbert spaces and the spectral isolation of cats guarantee the robustness of our proposal and open the door to studying improvements of the simulations using error-correction schemes [76,97]. Exploring systems with higher dimensionality would require additional Hamiltonian interactions (see the Supplemental Material [18]). Furthermore, the error correction capabilities of bosonic codes set the foundation to scalable $1+1D$ LGTs [102] and more involved symmetries, such as SU(2) LGTs [103–105] by incorporating additional bosonic codes.

We thank A. Eichler for critical reading of the manuscript and T. L. Heugel and C. Schweizer for fruitful discussions. J. d. P. was supported by the ETH Fellowship program (Grant No. 20-2 FEL-66). O. Z. acknowledges funding through SNSF Sinergia Grant No. CRSII5_198631 and from the Deutsche Forschungsgemeinschaft (DFG), Project No. 449653034.

*Corresponding author.
jdelpino@phys.ethz.ch

[1] K. G. Wilson, Confinement of quarks, Phys. Rev. D **10**, 2445 (1974).
[2] C. Gattringer and C. B. Lang, *Lect. Notes Phys.*, Lecture Notes in Physics Vol. 788 (Springer Berlin Heidelberg, Berlin, Heidelberg, 2010).
[3] Y. E. Kraus, Y. Lahini, Z. Ringel, M. Verbin, and O. Zilberberg, Topological States and Adiabatic Pumping in Quasicrystals, Phys. Rev. Lett. **109**, 106402 (2012).
[4] M. Verbin, O. Zilberberg, Y. E. Kraus, Y. Lahini, and Y. Silberberg, Observation of Topological Phase Transitions in Photonic Quasicrystals, Phys. Rev. Lett. **110**, 076403 (2013).
[5] M. Lohse, C. Schweizer, O. Zilberberg, M. Aidelsburger, and I. Bloch, A thouless quantum pump with ultracold bosonic atoms in an optical superlattice, Nat. Phys. **12**, 350 (2016).
[6] M. Lohse, C. Schweizer, H. M. Price, O. Zilberberg, and I. Bloch, Exploring 4D quantum Hall physics with a 2D topological charge pump, Nature (London) **553**, 55 (2018).
[7] O. Zilberberg, S. Huang, J. Guglielmon, M. Wang, K. P. Chen, Y. E. Kraus, and M. C. Rechtsman, Photonic topological boundary pumping as a probe of 4D quantum Hall physics, Nature (London) **553**, 59 (2018).
[8] I. Carusotto and C. Ciuti, Quantum fluids of light, Rev. Mod. Phys. **85**, 299 (2013).
[9] C. Gross and I. Bloch, Quantum simulations with ultracold atoms in optical lattices, Science **357**, 995 (2017).
[10] F. Ferri, R. Rosa-Medina, F. Finger, N. Dogra, M. Soriente, O. Zilberberg, T. Donner, and T. Esslinger, Emerging Dissipative Phases in a Superradiant Quantum Gas with Tunable Decay, Phys. Rev. X **11**, 041046 (2021).

[11] M. Schreiber, S. S. Hodgman, P. Bordia, H. P. Lüschen, M. H. Fischer, R. Vosk, E. Altman, U. Schneider, and I. Bloch, Observation of many-body localization of interacting fermions in a quasi-random optical lattice, Science **349**, 842 (2015).

[12] V. Goblot, A. Štrkalj, N. Pernet, J. L. Lado, C. Dorow, A. Lemaître, L. Le Gratiet, A. Harouri, I. Sagnes, S. Ravets, A. Amo, J. Bloch, and O. Zilberberg, Emergence of criticality through a cascade of delocalization transitions in quasiperiodic chains, Nat. Phys. **16**, 832 (2020).

[13] U. J. Wiese, Ultracold quantum gases and lattice systems: Quantum simulation of lattice gauge theories, Ann. Phys. (Amsterdam) **525**, 777 (2013).

[14] M. C. Bañuls, R. Blatt, J. Catani, A. Celi, J. I. Cirac, M. Dalmonte, L. Fallani, K. Jansen, M. Lewenstein, S. Montangero, C. A. Muschik, B. Reznik, E. Rico, L. Tagliacozzo, K. Van Acoleyen, F. Verstraete, U.-J. Wiese, M. Wingate, J. Zakrzewski, and P. Zoller, Simulating lattice gauge theories within quantum technologies, Eur. Phys. J. D **74**, 165 (2020).

[15] E. Zohar, J. I. Cirac, and B. Reznik, Quantum simulations of lattice gauge theories using ultracold atoms in optical lattices, Rep. Prog. Phys. **79**, 014401 (2016).

[16] E. Altman *et al.*, Quantum simulators: Architectures and opportunities, PRX Quantum **2**, 017003 (2021).

[17] J. Kogut and L. Susskind, Hamiltonian formulation of Wilson's lattice gauge theories, Phys. Rev. D **11**, 395 (1975).

[18] See Supplemental Material at http://link.aps.org/supplemental/10.1103/PhysRevLett.130.171901, which includes Refs. [17,19–36], for an overview of LGTs and their simplifications, a summary of bosonic error correction, the projection procedure onto the bosonic code limit, further evidence of distinct Rabi frequencies and multimode behaviour for strong 3WM, details on gauge invariance and numerical diagonalisation, and a proposal for the realisation of $\mathbb{Z}_2$ plaquette terms.

[19] C. Cohen-Tannoudji, B. Diu, and F. Laloe, *Quantum Mechanics, Volume 2*, edited by C. Cohen-Tannoudji, B. Diu, and F. Laloe (Wiley-VCH, 1986), Vol. 2, p. 626.

[20] D. B. Kaplan, A method for simulating chiral fermions on the lattice, Phys. Lett. B **288**, 342 (1992).

[21] J. D. Jackson and R. F. Fox, Classical electrodynamics, 3rd ed., Am. J. Phys. **67**, 841 (1999).

[22] V. May and O. Kühn, *Charge and Energy Transfer Dynamics in Molecular Systems* (Wiley, New York, 2003), 10.1002/9783527602575.

[23] U.-J. Wiese, An introduction to lattice field theory, *Foundations and New Methods in Theoretical Physics* (2009).

[24] M. A. Nielsen and I. L. Chuang, *Quantum Computation and Quantum Information: 10th Anniversary Edition* (Cambridge University Press, Cambridge, England, 2010), 10.1017/CBO9780511976667.

[25] O. Moussa, J. Baugh, C. A. Ryan, and R. Laflamme, Demonstration of Sufficient Control for Two Rounds of Quantum Error Correction in a Solid State Ensemble Quantum Information Processor, Phys. Rev. Lett. **107**, 160501 (2011).

[26] P. Schindler, J. T. Barreiro, T. Monz, V. Nebendahl, D. Nigg, M. Chwalla, M. Hennrich, and R. Blatt, Experimental repetitive quantum error correction, Science **332**, 1059 (2011).

[27] A. G. Fowler, M. Mariantoni, J. M. Martinis, and A. N. Cleland, Surface codes: Towards practical large-scale quantum computation, Phys. Rev. A **86**, 032324 (2012).

[28] M. H. Devoret and R. J. Schoelkopf, Superconducting circuits for quantum information: An outlook, Science **339**, 1169 (2013).

[29] A. Wipf, *Lect. Notes Phys*, Lecture Notes in Physics Vol. 100 (Springer Berlin Heidelberg, Berlin, Heidelberg, 2013), 10.1007/978-3-642-33105-3.

[30] L. Sun, A. Petrenko, Z. Leghtas, B. Vlastakis, G. Kirchmair, K. M. Sliwa, A. Narla, M. Hatridge, S. Shankar, J. Blumoff, L. Frunzio, M. Mirrahimi, M. H. Devoret, and R. J. Schoelkopf, Tracking photon jumps with repeated quantum non-demolition parity measurements, Nature (London) **511**, 444 (2014).

[31] D. Banerjee, M. Bögli, C. P. Hofmann, F.-J. Jiang, P. Widmer, and U.-J. Wiese, Interfaces, strings, and a soft mode in the square lattice quantum dimer model, Phys. Rev. B **90**, 245143 (2014).

[32] M. Sameti, A. Potočnik, D. E. Browne, A. Wallraff, and M. J. Hartmann, Superconducting quantum simulator for topological order and the toric code, Phys. Rev. A **95**, 042330 (2017).

[33] F. Jendrzejewski, T. Zache *et al.*, What are dynamical gauge fields? a simplistic introduction by an amo experimentalist, Authorea Preprints (2017), 10.22541/au.150663310.07882650.

[34] Z. Chen *et al.*, Exponential suppression of bit or phase errors with cyclic error correction, Nature (London) **595**, 383 (2021).

[35] A. Blais, A. L. Grimsmo, S. M. Girvin, and A. Wallraff, Circuit quantum electrodynamics, Rev. Mod. Phys. **93**, 025005 (2021).

[36] S. Krinner, N. Lacroix, A. Remm, A. Di Paolo, E. Genois, C. Leroux, C. Hellings, S. Lazar, F. Swiadek, J. Herrmann, G. J. Norris, C. K. Andersen, M. Müller, A. Blais, C. Eichler, and A. Wallraff, Realizing repeated quantum error correction in a distance-three surface code, Nature (London) **605**, 669 (2022).

[37] S. Chandrasekharan and U. J. Wiese, Quantum link models: A discrete approach to gauge theories, Nucl. Phys. **B492**, 455 (1997).

[38] O. Dutta, L. Tagliacozzo, M. Lewenstein, and J. Zakrzewski, Toolbox for Abelian lattice gauge theories with synthetic matter, Phys. Rev. A **95**, 053608 (2017).

[39] U. Borla, R. Verresen, F. Grusdt, and S. Moroz, Confined Phases of One-Dimensional Spinless Fermions Coupled to Z2 Gauge Theory, Phys. Rev. Lett. **124**, 120503 (2020).

[40] D. Gonzalez-Cuadra, A. Dauphin, P. R. Grzybowski, M. Lewenstein, and A. Bermudez, Dynamical Solitons and Boson Fractionalization in Cold-Atom Topological Insulators, Phys. Rev. Lett. **125**, 265301 (2020).

[41] A. Kitaev, Fault-tolerant quantum computation by anyons, Ann. Phys. (N.Y.) **303**, 2 (2003).

[42] N. Goldman, G. Juzeliunas, P. Ohberg, and I. B. Spielman, Light-induced gauge fields for ultracold atoms, Rep. Prog. Phys. **77**, 126401 (2014).

[43] N. Goldman and J. Dalibard, Periodically Driven Quantum Systems: Effective Hamiltonians and Engineered Gauge Fields, Phys. Rev. X **4**, 031027 (2014).
[44] S. Walter and F. Marquardt, Classical dynamical gauge fields in optomechanics, New J. Phys. **18**, 113029 (2016).
[45] P. Zapletal, S. Walter, and F. Marquardt, Dynamically generated synthetic electric fields for photons, Phys. Rev. A **100**, 023804 (2019).
[46] R. O. Umucalilar and I. Carusotto, Artificial gauge field for photons in coupled cavity arrays, Phys. Rev. A **84**, 043804 (2011).
[47] K. Fang, Z. Yu, and S. Fan, Realizing effective magnetic field for photons by controlling the phase of dynamic modulation, Nat. Photonics **6**, 782 (2012).
[48] V. Peano, C. Brendel, M. Schmidt, and F. Marquardt, Topological Phases of Sound and Light, Phys. Rev. X **5**, 031011 (2015).
[49] T. Ozawa, H. M. Price, A. Amo, N. Goldman, M. Hafezi, L. Lu, M. C. Rechtsman, D. Schuster, J. Simon, O. Zilberberg, and I. Carusotto, Topological photonics, Rev. Mod. Phys. **91**, 015006 (2019).
[50] J. P. Mathew, J. del Pino, and E. Verhagen, Synthetic gauge fields for phonon transport in a nano-optomechanical system, Nat. Nanotechnol. **15**, 198 (2020).
[51] J. del Pino, J. J. Slim, and E. Verhagen, Non-hermitian chiral phononics through optomechanically induced squeezing, Nature (London) **606**, 82 (2022).
[52] P. Hauke, D. Marcos, M. Dalmonte, and P. Zoller, Quantum Simulation of a Lattice Schwinger Model in a Chain of Trapped Ions, Phys. Rev. X **3**, 041018 (2013).
[53] C. Monroe, W. C. Campbell, L.-M. Duan, Z.-X. Gong, A. V. Gorshkov, P. W. Hess, R. Islam, K. Kim, N. M. Linke, G. Pagano, P. Richerme, C. Senko, and N. Y. Yao, Programmable quantum simulations of spin systems with trapped ions, Rev. Mod. Phys. **93**, 025001 (2021).
[54] M. Lewenstein, A. Sanpera, V. Ahufinger, B. Damski, A. Sen, and U. Sen, Ultracold atomic gases in optical lattices: Mimicking condensed matter physics and beyond, Adv. Phys. **56**, 243 (2007).
[55] D. Banerjee, M. Dalmonte, M. Müller, E. Rico, P. Stebler, U.-J. Wiese, and P. Zoller, Atomic Quantum Simulation of Dynamical Gauge Fields Coupled to Fermionic Matter: From String Breaking to Evolution After a Quench, Phys. Rev. Lett. **109**, 175302 (2012).
[56] L. Barbiero, C. Schweizer, M. Aidelsburger, E. Demler, N. Goldman, and F. Grusdt, Coupling ultracold matter to dynamical gauge fields in optical lattices: From flux attachment to $\mathbb{Z}_2$ lattice gauge theories, Sci. Adv. **5**, eaav7444 (2019).
[57] F. M. Surace, P. P. Mazza, G. Giudici, A. Lerose, A. Gambassi, and M. Dalmonte, Lattice Gauge Theories and String Dynamics in Rydberg Atom Quantum Simulators, Phys. Rev. X **10**, 021041 (2020).
[58] K. E. Ballantine, B. L. Lev, and J. Keeling, Meissner-like Effect for a Synthetic Gauge Field in Multimode Cavity QED, Phys. Rev. Lett. **118**, 045302 (2017).
[59] D. Marcos, P. Rabl, E. Rico, and P. Zoller, Superconducting Circuits for Quantum Simulation of Dynamical Gauge Fields, Phys. Rev. Lett. **111**, 1 (2013).
[60] D. Marcos, P. Widmer, E. Rico, M. Hafezi, P. Rabl, U. J. Wiese, and P. Zoller, Two-dimensional lattice gauge theories with superconducting quantum circuits, Ann. Phys. (N.Y.) **351**, 634 (2014).
[61] L. Homeier, C. Schweizer, M. Aidelsburger, A. Fedorov, and F. Grusdt, $\mathbb{Z}_2$ lattice gauge theories and Kitaev's toric code: A scheme for analog quantum simulation, Phys. Rev. B **104**, 085138 (2021).
[62] E. A. Martinez, C. A. Muschik, P. Schindler, D. Nigg, A. Erhard, M. Heyl, P. Hauke, M. Dalmonte, T. Monz, P. Zoller, and R. Blatt, Real-time dynamics of lattice gauge theories with a few-qubit quantum computer, Nature (London) **534**, 516 (2016).
[63] F. Görg, K. Sandholzer, J. Minguzzi, R. Desbuquois, M. Messer, and T. Esslinger, Realization of density-dependent Peierls phases to engineer quantized gauge fields coupled to ultracold matter, Nat. Phys. **15**, 1161 (2019).
[64] C. Schweizer, F. Grusdt, M. Berngruber, L. Barbiero, E. Demler, N. Goldman, I. Bloch, and M. Aidelsburger, Floquet approach to $\mathbb{Z}_2$ lattice gauge theories with ultracold atoms in optical lattices, Nat. Phys. **15**, 1168 (2019).
[65] B. Yang, H. Sun, R. Ott, H.-Y. Wang, T. V. Zache, J. C. Halimeh, Z.-S. Yuan, P. Hauke, and J.-W. Pan, Observation of gauge invariance in a 71-site Bose–Hubbard quantum simulator, Nature (London) **587**, 392 (2020).
[66] Z.-Y. Zhou, G.-X. Su, J. C. Halimeh, R. Ott, H. Sun, P. Hauke, B. Yang, Z.-S. Yuan, J. Berges, and J.-W. Pan, Thermalization dynamics of a gauge theory on a quantum simulator, Science **377**, 311 (2022).
[67] I. L. Chuang, D. W. Leung, and Y. Yamamoto, Bosonic quantum codes for amplitude damping, Phys. Rev. A **56**, 1114 (1997).
[68] B. M. Terhal, J. Conrad, and C. Vuillot, Towards scalable bosonic quantum error correction, Quantum Sci. Technol. **5**, 043001 (2020).
[69] A. Joshi, K. Noh, and Y. Y. Gao, Quantum information processing with bosonic qubits in circuit QED, Quantum Sci. Technol. **6**, 033001 (2021).
[70] W. Cai, Y. Ma, W. Wang, C.-L. Zou, and L. Sun, Bosonic quantum error correction codes in superconducting quantum circuits, Fundam. Res. **1**, 50 (2021).
[71] S. M. Girvin, Introduction to quantum error correction and fault tolerance, arXiv:2111.08894.
[72] Z. Leghtas, G. Kirchmair, B. Vlastakis, R. J. Schoelkopf, M. H. Devoret, and M. Mirrahimi, Hardware-Efficient Autonomous Quantum Memory Protection, Phys. Rev. Lett. **111**, 120501 (2013).
[73] B. Vlastakis, G. Kirchmair, Z. Leghtas, S. E. Nigg, L. Frunzio, S. M. Girvin, M. Mirrahimi, M. H. Devoret, and R. J. Schoelkopf, Deterministically encoding quantum information using 100-photon Schrödinger cat states, Science **342**, 607 (2013).
[74] C. Wang, Y. Y. Gao, P. Reinhold, R. W. Heeres, N. Ofek, K. Chou, C. Axline, M. Reagor, J. Blumoff, K. M. Sliwa, L. Frunzio, S. M. Girvin, L. Jiang, M. Mirrahimi, M. H. Devoret, and R. J. Schoelkopf, A Schrödinger cat living in two boxes, Science **352**, 1087 (2016).
[75] S. Puri, A. Grimm, P. Campagne-Ibarcq, A. Eickbusch, K. Noh, G. Roberts, L. Jiang, M. Mirrahimi, M. H. Devoret, and S. M. Girvin, Stabilized Cat in a Driven Nonlinear

Cavity: A Fault-Tolerant Error Syndrome Detector, Phys. Rev. X **9**, 041009 (2019).
[76] A. Grimm, N. E. Frattini, S. Puri, S. O. Mundhada, S. Touzard, M. Mirrahimi, S. M. Girvin, S. Shankar, and M. H. Devoret, The Kerr-Cat qubit: Stabilization, readout, and gates, Nature (London) **584**, 205 (2019).
[77] B. Hacker, S. Welte, S. Daiss, A. Shaukat, S. Ritter, L. Li, and G. Rempe, Deterministic creation of entangled atom–light Schrödinger-cat states, Nat. Photonics **13**, 110 (2019).
[78] D. J. Wineland, Nobel Lecture: Superposition, entanglement, and raising Schrödinger's cat, Rev. Mod. Phys. **85**, 1103 (2013).
[79] M. Bild, M. Fadel, Y. Yang, U. von Lüpke, P. Martin, A. Bruno, and Y. Chu, Schrödinger cat states of a 16-microgram mechanical oscillator, arXiv:2211.00449.
[80] D. Radić, S.-J. Choi, H. C. Park, J. Suh, R. I. Shekhter, and L. Y. Gorelik, Nanomechanical cat states generated by a dc voltage-driven cooper pair box qubit, npj Quantum Inf. **8**, 74 (2022).
[81] U. B. Hoff, J. Kollath-Bönig, J. S. Neergaard-Nielsen, and U. L. Andersen, Measurement-Induced Macroscopic Superposition States in Cavity Optomechanics, Phys. Rev. Lett. **117**, 143601 (2016).
[82] P. T. Cochrane, G. J. Milburn, and W. J. Munro, Macroscopically distinct quantum-superposition states as a bosonic code for amplitude damping, Phys. Rev. A **59**, 2631 (1999).
[83] B. Wielinga and G. J. Milburn, Quantum tunneling in a Kerr medium with parametric pumping, Phys. Rev. A **48**, 2494 (1993).
[84] D. F. Walls, Squeezed states of light, Nature (London) **306**, 141 (1983).
[85] A. Heidmann, R. J. Horowicz, S. Reynaud, E. Giacobino, C. Fabre, and G. Camy, Observation of Quantum Noise Reduction on Twin Laser Beams, Phys. Rev. Lett. **59**, 2555 (1987).
[86] R. W. Boyd and B. R. Masters, Nonlinear optics, third edition, J. Biomed. Opt. **14**, 029902 (2009).
[87] A. Penzkofer, A. Laubereau, and W. Kaiser, High intensity Raman interactions, Prog. Quantum Electron. **6**, 55 (1979).
[88] S. Mundhada, A. Grimm, J. Venkatraman, Z. Minev, S. Touzard, N. Frattini, V. Sivak, K. Sliwa, P. Reinhold, S. Shankar, M. Mirrahimi, and M. Devoret, Experimental Implementation of a Raman-Assisted Eight-Wave Mixing Process, Phys. Rev. Appl. **12**, 054051 (2019).
[89] L. A. Kanari-Naish, J. Clarke, S. Qvarfort, and M. R. Vanner, Two-mode schrödinger-cat states with nonlinear optomechanics: Generation and verification of non-gaussian mechanical entanglement, Quantum Sci. Technol. **7**, 035012 (2022).
[90] S. Ramelow, L. Ratschbacher, A. Fedrizzi, N. K. Langford, and A. Zeilinger, Discrete Tunable Color Entanglement, Phys. Rev. Lett. **103**, 253601 (2009).
[91] A. S. Coelho, F. A. S. Barbosa, K. N. Cassemiro, A. S. Villar, M. Martinelli, and P. Nussenzveig, Three-color entanglement, Science **326**, 823 (2009).
[92] B. Abdo, A. Kamal, and M. H. Devoret, Non-degenerate, three-wave mixing with the Josephson ring modulator, Phys. Rev. B **87**, 014508 (2012).
[93] I. Carusotto and C. Ciuti, Quantum fluids of light, Rev. Mod. Phys. **85**, 299 (2013).
[94] N. C. Zambon, S. R. K. Rodriguez, A. Lemaitre, A. Harouri, L. L. Gratiet, I. Sagnes, P. St-Jean, S. Ravets, A. Amo, and J. Bloch, Parametric instability in coupled nonlinear microcavities, Phys. Rev. A **102**, 023526 (2019).
[95] M. Frimmer and L. Novotny, The classical Bloch equations, Am. J. Phys. **82**, 947 (2014).
[96] D. Hälg, T. Gisler, E. C. Langman, S. Misra, O. Zilberberg, A. Schliesser, C. L. Degen, and A. Eichler, Strong Parametric Coupling Between Two Ultracoherent Membrane Modes, Phys. Rev. Lett. **128**, 094301 (2022).
[97] M. Mirrahimi, Z. Leghtas, V. V. Albert, S. Touzard, R. J. Schoelkopf, L. Jiang, and M. H. Devoret, Dynamically protected cat-qubits: A new paradigm for universal quantum computation, New J. Phys. **16**, 045014 (2014).
[98] T. Kanao, S. Masuda, S. Kawabata, and H. Goto, Quantum Gate for a Kerr Nonlinear Parametric Oscillator Using Effective Excited States, Phys. Rev. Appl. **18**, 014019 (2022).
[99] L. Gilles, B. M. Garraway, and P. L. Knight, Generation of nonclassical light by dissipative two-photon processes, Phys. Rev. A **49**, 2785 (1994).
[100] T. L. Heugel, M. Biondi, O. Zilberberg, and R. Chitra, Quantum Transducer Using a Parametric Driven-Dissipative Phase Transition, Phys. Rev. Lett. **123**, 173601 (2019).
[101] T. L. Heugel, A. Eichler, R. Chitra, and O. Zilberberg, The role of fluctuations in quantum and classical time crystals, arXiv:2203.05577.
[102] Z. Yao, C. Liu, P. Zhang, and H. Zhai, Many-body localization from dynamical gauge fields, Phys. Rev. B **102**, 104302 (2020).
[103] D. Banerjee, M. Bögli, M. Dalmonte, E. Rico, P. Stebler, U. J. Wiese, and P. Zoller, Atomic Quantum Simulation of U(N) and SU(N) Non-Abelian Lattice Gauge Theories, Phys. Rev. Lett. **110**, 125303 (2012).
[104] E. Zohar, J. I. Cirac, and B. Reznik, Cold-Atom Quantum Simulator for SU(2) Yang-Mills Lattice Gauge Theory, Phys. Rev. Lett. **110**, 125304 (2013).
[105] L. Tagliacozzo, A. Celi, P. Orland, M. W. Mitchell, and M. Lewenstein, Simulation of non-Abelian gauge theories with optical lattices, Nat. Commun. **4**, 2615 (2013).